CHARGE-EXCHANGE PROCESSES AT MARS: ENAS AND X-RAYS

Kallio[1], E., and M. Holmström[2]

[1] *Finnish Meteorological Institute, Helsinki, Finland*
[2] *Swedish Institute of Space Physics, Kiruna, Sweden.*

1. Charge-exchange processes

As was established by earlier missions, and confirmed recently by the Mars Global Surveyor, Mars does not possess an intrinsic dipole magnetic field but only local crustal magnetizations [*Acuna et al.*, 1998]. The local field plays a role in the solar wind interaction only over limited regions, while for the overall interaction picture, the solar wind interacts directly with the Martian ionosphere, exosphere, and upper atmosphere. As a result of the low gravity on Mars, the neutral density can reach 10^4–10^6 cm^{-3} in the interaction region where the main plasma boundaries, the bow shock and the magnetopause are located.

The co-existence of these two components, the solar wind plasma and the planetary neutral gas, results in a strong interaction between them. One of the fundamental collisional interactions is the charge-exchange (CX) process between the energetic ion, A^+, and the cold atmospheric gas, M:

$$A^+(energetic) + M(cold) \rightarrow A(energetic) + M^+(cold), \quad [1]$$

that produces energetic neutral atoms, A, and an ionized gas particle. Examples of CX processes of special importance at Mars are the processes

$$H_{SW}^+ + H \rightarrow H_{SW} + H^+, \quad [2a]$$
$$H_{SW}^+ + O \rightarrow H_{SW} + O^+, \quad [2b]$$
$$H_{pickup}^+ + H \rightarrow H_{pickup} + H^+, \quad [2c]$$
$$O_{pickup}^+ + H \rightarrow O_{pickup} + H^+. \quad [2d]$$

Above, the first three processes 2a-c produce fast hydrogen ENAs, H-ENAs. The process 2d produces fast oxygen atoms, O-ENAs. Subscripts SW and pickup refer to particles originating from the Sun and from the planetary atmosphere or exosphere, respectively. The important feature of these CX processes is that the velocity of the formed ENA is about the same as the velocity of the initial energetic (E>>1 eV) fast ion. The formed ENAs therefore carry practically uninterrupted information about the properties of the ions from the site at which they were formed.

The solar wind also contains heavy multiple charged ions, for example, O^{6+} ions. The charge-exchange with a multiple charged ion, say an n times charged ion X^{n+}, and a neutral, M, is a source of X-ray photons, *hf*:

$$X^{n+} + M \rightarrow X^{*(n-1)+} + M^+ \rightarrow X^{(n-1)+} + M^+ + hf, \quad [3]$$

where the superscript * refers to the exited state. From a measuring point of view, the CX process that produces ENAs (Equation 1) and the CX process that produces X-rays (Equation 3) are of importance because both ENAs and X-rays provides the possibility to obtain a global image of the interaction, as will be illustrated later.

2. The solar wind - atmosphere coupling

Near-Mars space is strikingly different from near-Earth space because of the absence of a substantial intrinsic magnetic field of Mars. Without the magnetic cavity of a magnetosphere to shield the upper atmosphere from the on-coming solar wind, Mars is subject to comet-like

atmosphere erosion processes and solar wind-induced current systems. Both previous missions to Mars (especially Phobos-2 mission) and experience gained in orbit around another weakly magnetized planet, Venus, on the Pioneer Venus Orbiter, have given information about how the Martian upper atmosphere interacts with the solar wind, and about the possible consequences of the interaction. In particular, observations suggest that the scavenging of planetary ions may have resulted in the removal of ~1 m of surface water over 4.5 billion years [*Lundin et al.*, 1991]. More detailed studies [*Zhang et al.*, 1993], that take into account the variability of the ionosphere throughout the planetary history, give a much higher (~30 m) equivalent depth of water, that has escaped due to the solar wind interaction process.

The current atmospheric conditions on Mars indicate that water does not exist on the surface in any significant amount (an equivalent water layer is 15 μm deep [*Farmer et al.*, 1977]). On the other hand, independent analyses of several features of the planet, such as geomorphologic features, SNC meteorites, isotopic abundance and volcanic activity, indicate that water existed in the past on the Martian surface (see, for example, *McKay and Stoker*, 1989). Thus we come to the problem of Mars dehydration. Where is the Martian water? Is it lost or frozen and buried? If it is the former, what could produce an effective enough escape mechanism? If the latter, where is the water stored?

Another problem of the solar wind - atmosphere coupling that has not been explored experimentally concerns the energetic consequences for the Martian atmosphere of the lack of a Martian dipole field of any importance. Kinetic and test-particle models of the Mars-solar wind interaction [*Brecht*, 1997; *Kallio et al.*, 1997; *Kallio and Janhunen*, 2001] suggest that solar wind absorption by the Martian atmosphere may be an important energy source for the upper atmosphere. The ENAs generated as a product of the solar wind interaction further enhance the deposition of solar wind energy [*Kallio and Barabash*, 2000, 2001] and, at the same time, provide a means of "imaging" the solar wind interaction.

The Martian atmosphere, although thin, alters the incoming energetic solar wind by (*a*) generation of ionospheric currents that partially deflect the ion flow around the Martian ionosphere, (*b*) "mass loading" the solar wind with planetary ions produced mainly by photoionization, and solar wind electron impact ionization of the atmospheric gases, and (*c*) undergoing charge-transfer (charge-exchange) interactions with the solar wind ions. According to the models, some of the solar wind ions (mainly H^+ and He^{++} ions) directly impact Martian upper atmosphere near its exobase (at ~180 km altitude) because their gyroradii are too large to behave as a deflected "fluid" in the subsolar magnetosheath (see *Brecht*, 1997, and *Kallio and Janhunen*, 2001) or because they are partially thermalized by the bow shock. Others undergo charge-exchange reactions with ambient exospheric and thermospheric neutrals, particularly hydrogen and helium and then impact the exobase as ENAs [*Kallio et al.*, 1997]. In both cases, solar wind energy is directly deposited into the upper atmosphere resulting in increasing ionization rates and UV emissions.

When the effects of such ENA precipitation was studied by Monte Carlo simulations, the precipitating hydrogen atoms was estimated to increase the ionization rate by about 1% in comparison with ionization rates due to extreme ultraviolet radiation under typical solar wind conditions [*Kallio and Barabash*, 2000, 2001]. This effect is comparable to, or even stronger than similar effects caused by the O^+ and H^+ precipitation [*Luhmann and Kozyra*, 1991; *Brecht*, 1997; *Kallio and Janhunen*, 2001]. The results also indicate that a substantial part of the incoming particles is scattered back from the Martian atmosphere resulting in an ENA hydrogen albedo. Imaging these particles would visualize the spots or regions of the most intense ENA precipitation.

While the energy transfer associated with the proton or ENA precipitation exceeds the one from the O^+ precipitation, it is the oxygen ions that causes massive sputtering of the atmosphere [*Luhmann and Kozyra*, 1991; *Luhmann et al.*, 1992]. The sputtering caused by O^+ ions has been estimated to results in the escape of 0.1–0.5 kg/s of oxygen atoms [*Luhmann*

and Bauer, 1992]. That is on the same level as the non-thermal escape of the hot oxygen atmospheric component.

3. Sources of Energetic Neutral Atoms at Mars

ENAs are produced by charge-exchange between the Martian exosphere containing H, H_2, He and O, and the different plasma populations such as (1) the supersonic solar wind [*Kallio et al.*, 1997; *Holmström et al.*, 2001], (2) the shocked solar wind [*Kallio et al.*, 1997; *Holmström et al.*, 2001], and (3) accelerated planetary ions [*Barabash et al.*, 2001; *Lichtenegger et al.*, 2001]. The Phobos moon's atmosphere (4) also interacts with both the supersonic and the shocked solar wind resulting in ENA generation [*Mura et al.*, 2001]. The energetic O^+ ions picked up by the plasma flow incident on the atmosphere sputter or backscatter oxygen, CO_2 and its fragments [*Luhmann and Kozyra*, 1991; *Luhmann et al.*, 1992]. In addition, the back-scattered atoms form an oxygen ENA albedo (5). The intensity of these emissions directly determines the efficiency of the atmospheric erosion. The precipitating protons and hydrogen ENAs can also be scattered back, forming a hydrogen ENA albedo (6) [*Kallio and Barabash*, 2001; *Holmström et al.*, 2001].

3.1. Hydrogen ENAs

The supersonic solar wind upstream of the bow shock can experience charge-exchange with the Martian hydrogen exosphere (Equations 2a and 2b) over very long distances resulting in a narrow (~10°) anti-sunward beam of ENAs with the energy of the bulk flow of the solar wind.

Figure 1 shows simulated directional hydrogen ENA flux produced by solar wind protons. The H-ENA flux was integrated over energy as a function of two spherical angles at four positions (1-4) along the orbit of a virtual spacecraft, which orbit looks like the orbit of the Mars Express spacecraft. In this fish-eye projection, the look direction (the polar coordinate axis) is toward the Sun. In Figure 1 the distance from the Sun, that is at the center at each four images, gives the polar angle, θ. The azimuth angle, φ, measured around the polar axis, was chosen to be zero for the center of Mars. The ENA fish-eye pictures illustrates the integrated fluxes in several directions for the energy range E>100 eV based on an axially symmetric model for the solar wind proton flow around Mars. Note than in Figure 1 the ENA flux at polar angles less than 15° was put to zero to mimic ENA observations: An ENA instrument cannot look directly toward the Sun because of the EUV radiation from the Sun.

Figure 1 illustrates how an H-ENA image evolves when the vantage point moves from the apocenter (position 4) toward the pericenter (position 1). The maximum fluxes are obtained at $\varphi = 0°$, that is, between the Sun and the center of Mars. The spread of the distribution to non-zero φ depends on the proton temperature: a zero proton temperature would give non-zero fluxes only on the $\varphi = 0°$ line, that is, on the line between the Sun and Mars. Non-zero proton temperature give, instead, non-zero fluxes at other φ angles as well, as is the case in Figure 1. Note that the used plasma model is axially symmetric and therefore the solution on the hemisphere $\varphi = 0°–180°$ and $\varphi = 180°–360°$ is symmetric.. The value of the maximum ENA flux depends on the flux of the solar wind protons, the shape and the distance of the bow shock and the magnetopause, as well as the proton parameters downstream of the bow shock. The produced ENA fluxes generated from the shocked solar wind are most sensitive to the neutral hydrogen distribution controlled by the exobase temperature and the position of the boundary separating the solar wind and planetary plasmas [*Holmström et al.*, 2001]. The ENA images display the entire interaction region and can be converted into global distributions of the proton flow and neutral gas using extracting diagnostic methods similar to the one developed for Earth [*Roelof and Skinner*, 2000].

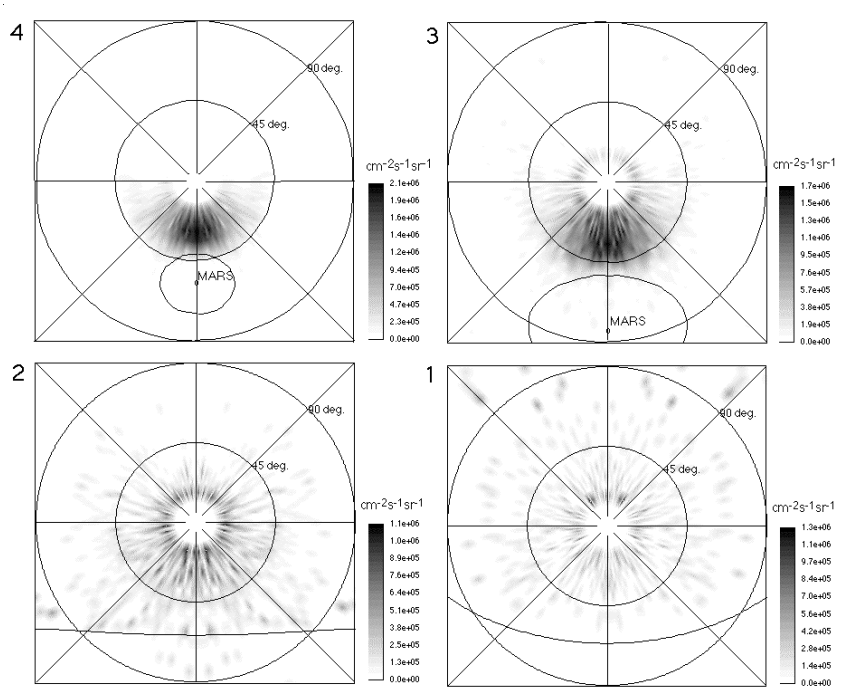

Figure 1. Simulated hydrogen ENA particle fluxes at four vantage points No 4-1 from the apocenter (point No 4) to the pericenter (point No 1). The look direction (the polar coordinate axis) is toward the Sun, that is at the center of the images. The inner (outer) circle around the Sun represents the polar angle, θ, of 45° (90°). The lines originating from the center of the figures represent constant azimuth angles, φ. The ENAs in the region θ <15° are blocked.

The Martian hydrogen corona provides another source of fast H^+ ions. The accelerated planetary protons, originating from ionization of the hydrogen corona, also charge-exchange with the exospheric gas, resulting in planetary hydrogen ENA emissions (Equations 2c). The H-ENAs produced from these pick-up H^+ ions differ from the H-ENAs produced from the shocked solar wind protons in energy because the pick-up protons can gain an energy up to four times the solar wind energy [*Lichtenegger et al.,* 2001].

3.2. Oxygen ENAs

The ASPERA/Phobos-2 observations of the plasma energization inside the Martian magnetosphere have shown the existence of two basic ion populations: The tail beams of H^+ and O^+ with energy 1–3 keV, and the outflowing ionospheric ions with energy 10–100 eV near the tail flanks [*Lundin et al.,* 1993]. The related ENA flux has been estimated to be 10^3 $cm^{-2}s^{-1}keV^{-1}$ for the energy range 1–10 keV, and up to 10^5 $cm^{-2}s^{-1}keV^{-1}$ for lower energies, 10–100 eV [*Barabash et al.,* 1995a].

The ENA signal associated with the pick-up oxygen (see Equation 2d) was recently investigated in detail by solving numerically the kinetic equation to obtain the global distribution of oxygen ions [*Barabash et al.*, 2001]. The obtained O^+ distribution, as recent self-consistent kinetic simulations [*Kallio and Janh*unen, 2002], illustrated high asymmetry with respect to the direction of the interplanetary electric field $\mathbf{E}_{SW} = -\mathbf{U}_{SW}x\mathbf{B}_{SW}$. When the derived O^+ distribution was converted to the corresponding O-ENA flux it was found that the fluxes of the oxygen ENAs could reach 10^4 $cm^{-2}s^{-1}sr^{-1}eV^{-1}$ and that it fully reflects the morphology of the oxygen population demonstrating that O-ENAs provides a way to determine the instantaneous oxygen escape rate.

Figure 2 gives an example of the simulated O-ENA images for the energy range 0.1–1.65 keV. The figure shows the vantage points and the corresponding ENA images in the fish-eye

projection for two vantage points, No 2 and No 4. The projection is a polar one with the radius being the angle to the axis pointing towards the center of Mars and the polar angle the angle to the solar direction in the plane perpendicular to the planetary center direction. The chosen energy range covers the main oxygen ion population near Mars, and it still makes the result relevant to modern ENA instrumentation. The angular resolution for the line-of-sight grid was 2.5°–5°. The field of view is 120° to cover the entire interaction region. As expected, O-ENA emissions are concentrated close to the planetary surface where the neutral density is highest reflecting also the strong asymmetry observed in the ion distribution. Note that Figure 2 (point No 2) shows a strong jet of oxygen ENA coming out from the subsolar point where the electric and magnetic field configuration effectively accelerates newly formed planetary ions. The tailward flow is also clearly reproduced (Figure 2, point 4). In contrast, when simulations for vantage points on the +Y axis at the distance 3 R_M were made, only very weak O-ENA fluxes were obtained (figures not shown). Finally, simulations for a higher energy band of 1.65–5.0 keV showed that O-ENA image morphology is similar to the ones for the lower energy band but that fluxes are two orders of magnitude weaker (figures not shown).

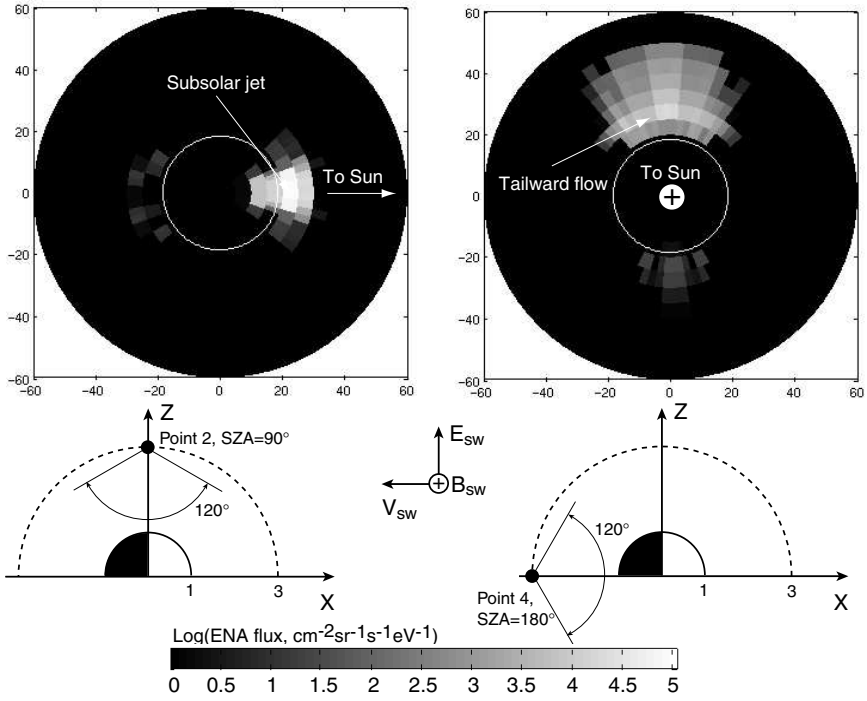

Figure 2. Oxygen ENA images for two vantage points: At the terminator plane (point No 2, the left image) and at the midnight (point No 4, the right image). The energy range is 0.1–1.65 keV. The position of the vantage points are shown in the inserts as well as the direction of the convective electric field ($\mathbf{E}_{sw}$) in the solar wind, and the interplanetary magnetic field ($\mathbf{B}_{sw}$). Both vantage points are on the OXZ plane.

3.3. ENAs associated with Phobos

Several experiments on the Phobos-2 mission observed brief plasma disturbances when the spacecraft crossed the Phobos orbit (see review and references by *Barabash,* 1995b). They could be related to Phobos' neutral gas torus, resulting from outgassing from the moon. The solar wind plasma experience charge-exchange with Phobos "atmosphere" and the neutral torus, resulting in ENA emissions. Assuming an outgassing rate of 10^{23} s^{-1} the associated H-ENA flux has been estimated to be on the order of 10^3–10^4 $cm^{-2}s^{-1}keV^{-1}$ for the shocked

solar wind plasma and up to 10^6 $cm^{-2}s^{-1}keV^{-1}$ for the solar wind beam [*Mura et al.*, 2001]. Due to solar radiation, the Phobos ENAs and the Phobos torus ENAs can only be observed when the moon is in the magnetosheath and the plasma flow deviates strongly from the anti-solar direction.

4. Mars as an X-ray source

There are several mechanisms that can generate X-ray emissions from Mars. Apart from charge-exchange between solar wind ions and Mars' exosphere (Equation 3), there is also fluorescent and elastic scattering of solar X-rays by Mars' atmosphere.

Mars has been suggested to emit significant X-ray fluxes from charge-exchange [*Cravens*, 2000]. Figure 3 shows an example of a computer simulated X-ray image of the solar wind-Mars interaction [*Holmström et al.*, 2001]. The maximum directional fluxes was found to be on the order of 10^6 eV/(cm^2 sterad s) and depends on the solar wind conditions and view direction. The energy of the emitted X-rays is mostly below 1 keV.

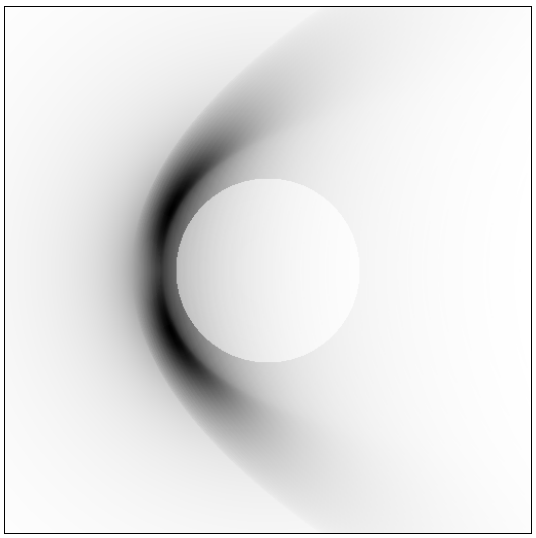

Figure 3. A computer simulated image of Martian X-ray emissions from charge-exchange between solar wind ions and Mars' exosphere. The view direction is perpendicular to the Mars-Sun line, with the Sun to the left. Mars is seen as a white disc.

Estimates of Martian X-ray emissions from fluorescent and elastic scattering of solar X-rays by the planets' atmosphere [*Cravens and Maurellis*, 2001] is larger, but on the same order of magnitude as that from charge-exchange. Due to the uncertainties in the estimates of the X-ray fluxes emitted by the different mechanisms, it is still an open question which of the mechanisms is the dominating one. When future observations settle this issue, resulting in more precise models for the X-ray emissions, X-ray imaging promise to be a complement to ENA imaging in providing global information about the near-Mars space. The recent announcement of the detection, and imaging, of X-ray emissions from Venus by the X-ray telescope Chandra [*Dennerl*, 2001] makes it plausible that X-ray emissions from Mars will also be observed soon.

Finally, although the X-ray generation mechanism is similar for comets and Mars it is interesting to note to following differences between these X rays sources. For comets, due to very large spatial scales of the neutral gas distribution, the heavy ion component of the solar wind is totally depleted while moving through the cometary coma (that is the reason of the absent of the X-ray emission from the tail) and the peak X-ray flux is determined by the heavy ion density. In contrast, at Mars, the scale of the neutral gas distribution is small in comparison with the charge-exchange distance and a very small fraction of the solar wind ions is lost during the interaction.

5. Future

5.1. ENA imaging of the Martian environment

ENA images provide information in two ways. First of all, they reveal morphological features of the ENA sources, such as the location of boundaries and their relative sizes. ENA images are useful, in particular, for investigating different types of asymmetries expected for the plasma flow near Mars [*Dubinin et al.,* 1996]. The ENA images of the escaping plasma display globally and instantaneously the size and geometry of the outflowing plasma region. These characteristics are particularly important for calculations of the total non-thermal plasma outflow. For instance, the local ion measurements made using two instruments, ASPERA and TAUS, during the Phobos-2 mission gave comparable ion fluxes. However, different assumptions made regarding the outflow region geometry (mass-loading boundary, plasma sheet) resulted in significant differences in the total outflow rate estimations, 0.5–1.0 kg/s [*Lundin et al.,* 1989] and 0.15 kg/s [*Verigin et al.,* 1991]. One of the reasons for this was ambiguity in separating spatial and temporal variations, which is typical for local plasma measurements. Global and instantaneous observations of the outflowing plasma region morphology to be made via ENA imaging would help to resolve this issue that is important for understanding the planetary atmospheric evolution.

Secondly, beside morphological features, ENA images carry an ample amount of quantitative information about both the planetary plasma and neutral environments. By applying inversion techniques to images of the shocked solar wind, quantitative models for the neutral gas profiles, namely, the exobase densities and temperatures, and global proton plasma distributions, namely, the flow geometry, bulk velocity, density, and temperature can be derived.

Mars Global Surveyor measurements has indicated that the atmospheric density can vary noticeably [*Bougher et al*., 2001]. Global ENA imaging of the interaction offers the promise of separating the spatial and temporal variations of the atmosphere - solar wind interaction. Apart from imaging, the measurements of ENA flux from certain directions provide a diagnostic tool for plasma-atmosphere coupling studies. Precipitating ENAs and ENA albedo (back-scattered oxygen) are direct manifestation of such an interaction.

5.2. X-ray imaging

As pointed out in Section 4, a very small fraction of the solar wind ions is lost during the Mars-solar wind interaction at charge-exchange processes. In most regions around Mars this fraction amounts to just a few percent and the loss can be disregarded. That means that comets' X-ray emissions can be used to probe the solar wind while at Mars it provides a natural way to probe the planetary environment.

X-ray imaging of the near-Mars space therefore opens up opportunities to remotely diagnose the structure of the solar wind interaction region. If assume that the neutral gas distribution is a known parameter, the deconvolution of X-ray images, for example, via forward-modeling, would provide the global distribution of the solar wind heavy ions. This, in turn, can be converted to the proton distribution. Moreover, it would give extra information about the accuracy of the magnetic field models used because the motion of the heavy ions which could be considered as test particles is governed by the Lorentz force. Since X-ray imaging can be performed in the undisturbed solar wind, simultaneous monitoring of the minor ion density and composition is also possible.

5.3. Mars missions

ESA's Mars Express spacecraft includes an ENA instrument, ASPERA-3, to perform the first ENA imaging of another planet in the low energy (E<60 keV) range. The ASPERA-3 experiment makes it possible to image all of the aforementioned H- and O-ENA sources. The Japanese Nozomi, launched to Mars in 1998, is concentrating on plasma measurements and does not include in its payload any ENA instrumentation.

However, Mars Express and Nozomi are highly complementary missions. Nozomi with its comprehensive plasma payload provides the necessary local context for the remote ENA measurements from Mars Express. Two simultaneous plasma observations make it possible to distinguish spatial and temporal variations in the magnetospheric plasma. Particularly promising configurations would occur when one of the satellites is in the solar wind while the second one is in the near-Mars environment. In this case one can investigate the instantaneous response of the system against variations in the solar wind. Knowing the system's dynamical behavior one can evaluate the evolutionary effects more precisely.

Acknowledgment. The authors thank Dr. Stas Barabash for his help in preparing this paper.

Submitted: Jan 14, 2002. 2nd version.
Contact person: Esa Kallio (Esa.Kallio@fmi.fi).

6. References

Acuna, M. H., et al., Magnetic Field and Plasma Observations at mars: Initial Results of the Mars Global Surveyor mission, Science, 279, 1676, 1998.

Barabash, S., et al., Diagnostic of energetic neutral particles at Mars by the ASPERA-C instrument for the Mars 96 mission, Adv. Space Res., 16, (4)81, 1995a.

Barabash, S., Satellite observations of the plasma - neutral coupling near Mars and the earth, IRF Scientific Report, 228, 1995b.

Barabash, S., M. Holmström, A. Lukyanov, and E. Kallio, Energetic neutral atoms at Mars IV: Imaging of planetary oxygen, submitted to J. Geophys. Res., 2001.

Bougher, S. W., Engel, S., Hinson, D. P., and Forbes, J. M., Mars Global Surveyor Radio Science electron density profiles: Neutral atmosphere implications, Geophys. Res. Lett., 16, 3091-3094, 2001.

Brecht, S.H., Solar Wind proton deposition into the Martian atmosphere, J. Geophys. Res. 102, 11,287, 1997.

Cravens, T. E., X-ray emission from comets and planets, Adv. Space Res., 26, 1443-1451, 2000.

Cravens, T. E., A. N. Maurellis, X-ray emission from scattering and fluorescence of solar x-rays at Venus and Mars. Geophys. Res. Lett, 28, 3043-3046, 2001.

Dennerl, K., Discovery of X-rays from Venus with Chandra. In "High Energy Universe at Sharp Focus: Chandra Science." proceedings of a conference held in St. Paul, MN, 16-18 July 2001. ASP Conference Series, 2001.

Dubinin, E., et al., Plasma characteristics of the boundary layer in the Martian magnetosphere, J. Geophys. Res., 101, 27,061, 1996.

Farmer, C. B., et al., Mars: Water vapour observations from the Viking orbiters, J. Geophys. Res., 82, 4225, 1977.

Holmström, M., S. Barabash, and E. Kallio, X-ray imaging of the solar wind-Mars interaction. Geophys. Res. Lett, 28, 1287-1290, 2001.

Holmström, M., S. Barabash, and E. Kallio, Energetic neutral atoms at Mars I: Imaging of solar wind protons, accepted to be published in J. Geophys. Res., 2001.

Farmer, C. B., et al., Mars: Water vapour observations from the Viking orbiters, J. Geophys. Res., 82, 4225, 1977.

Kallio, E., J. G. Luhmann, and S. Barabash, Charge exchange near Mars: The solar wind absorption and energetic neutral atom production, J. Geophys. Res. 102, 22,183, 1997.

Kallio, E., and S. Barabash, On the elastic and inelastic collisions between the precipitating energetic hydrogen atoms and the Martian atmospheric neutrals, J. Geophys. Res., 105, 24973-24996, 2000.

Kallio, E., and S. Barabash, Atmospheric effects of precipitating energetic hydrogen atoms to the Martian atmosphere, J. Geophys. Res., 106, 165-177, 2001.

Kallio, E. and P. Janhunen, Atmospheric effects of proton precipitation in the Martian atmosphere and its connection to the Mars-solar wind interaction, J. Geophys. Res., 106, 5617, 2001.

Kallio, E. and P. Janhunen, Ion escape from Mars in a quasi-neutral hybrid model., J. Geophys. Res., *in press*, 2002.

Lichtenegger, H., H. Lammer, and W. Stumptner, Energetic neutral atoms at Mars III: Flux and energy distribution of planetary energetic H atoms, submitted to J. Geophys. Res., 2001.

Luhmann, J. G. and J. U. Kozyra, Dayside pickup oxygen ion precipitation at Venus and Mars: Spatial distributions, energy deposition and consequences, J. Geophys. Res., 96, 5457, 1991.

Luhmann, J. G., et al., Evolutionary impact of sputtering of the Martian atmosphere by O+ pickup ions, Geophys. Res. Lett., 19, 2151, 1992.

Luhmann, J. G., and S. J. Bauer, Solar wind effects on atmospheric evolution at Venus and Mars, in Venus and Mars: Atmospheres, ionospheres, and solar wind interactions, AGU monograph, 66, 417-430, 1992.

Lundin, R., et al., First measurements of the ionospheric plasma escape from Mars, Nature, 341, 609, 1989.

Lundin, R., et al., ASPERA observations of Martian magnetospheric boundaries, in Plasma environments of non-magnetic planets, ed. by T. I. Gombosi, Pergamon Press, p. 311, 1993.

McKay , C. P., and C. R. Stoker, The early environment and its evolution on Mars: implications for life, Rev. of Geophys., 27, 189, 1989.

Mura, A., A. Milillo, S. Orsini, E. Kallio, and S. Barabash, Energetic neutral atoms at Mars II: Energetic Neutral Atom production near Phobos, submitted to J. Geophys. Res., 2001.

Roelof, E. C., and A. J. Skinner, Extraction of ion distributions from magnetospheric and EUV images, Space Sci. Rev., 91, 437-459, 2000.

Verigin, M., et al., On the problem of the Martian atmosphere dissipation: PHOBOS 2 TAUS spectrometer results, J. Geophys. Res., 96, 19,315 - 19,320, 1991.

Zhang, M. H. G., J. G. Luhmann, S. W. Bougher, and A. F. Nagy, The ancient oxygen exosphere of Mars: Implication for atmospheric evolution, J. Geophys. Res., 98, 10,915-10,923, 1993.